The energy efficiency evaluation of hybrid energy storage system based on ultra-capacitor and $LiFePO_4$ battery

ZHIWEI WU, JIANLONG ZHANG, LEI JIANG, HONGJIE WU, CHENGLIANG YIN

National Engineering Laboratory for Automotive Electronic Control Technology

Shanghai Jiao Tong University

Dong Chuang Road 800, Shanghai, China

E-mail: Phd_knight@sjtu.edu.cn

Abstract: - Due to the unique characteristics of frequently charging and discharging at large power of battery in Hybrid electric vehicles and electric vehicles application, this paper focuses on combining ultra-capacitor with $LiFePO_4$ battery to improve the performance of energy storage system. Based on the experiment, the efficiency map of the ultra-capacitor and the $LiFePO_4$ battery are obtained. With the ultra-capacitor's support, the battery can be relieved from the stress of peak power and the efficiency of the battery can be improved. The inductor input half bridge bidirectional DC-DC converter employed as the interface of the ultra-capacitor and battery results in the extra energy loss. The DC-DC efficiency research is a key point. Based on the hybrid energy storage system (HESS) architecture, the DC-DC model has been built to acquire the bidirectional DC-DC efficiency map. Finally, the NEDC cycle simulation results demonstrate that compared with the battery only system, the EV with the HESS system is more efficient and the energy efficiency improvement is 3.5%. The voltage variation of the DC link in HESS is less than that in the battery only system.

Key-Words: - Ultra-capacitor, $LiFePO_4$ battery, HESS, Bidirectional DC-DC converter

NOMENCLATURE
DC-DC : direct current-direct current
HESS : hybrid energy storage system
HEVs : Hybrid electric vehicles
EVs : electric vehicles
HPPC : Hybrid Pulse Power Characterization
Voc : open circuit voltage
SOC : State of Charge
ESR : equivalent series resistance
IGBT : insulated gate bipolar transistor

1 Introduction

Facing the current oil crisis and environmental issues protection, the fuel efficiency of the traditional petrol fuel powered vehicles is not satisfactory especially during idling and acceleration. Furthermore, the emission policy will be strict. In these situations, Hybrid electric vehicles (HEVs) and electric vehicles (EVs) have become the focus nowadays. Some features of HEV, including down-sized engine, idling elimination, regenerative brake, low-speed electric propulsion and proper control strategy, etc., improve its fuel economy [1, 2, 3, 4].

Table 1. Development status of energy storage components [5]

#	chemistry	Specific energy Wh/kg	Specific power W/kg
1	Pb-acid	40	100
2	NIMH	80	700
3	Li-ion Energy	150	900
4	Ultra-capacitor	5.6	11000

The HEVs and EVs have high demand on the specific power of the energy storage system. In this investigation, ultra-capacitor (high power, fast response) has been combined with batteries (relatively slow response) to improve the life and performance of the system. The development status of energy storage components is shown in Table 1. Compared with battery, the ultra-capacitor has low specific energy. However, the specific power is excellently high. The ultra-capacitor use electrolyte

solutions but have even greater capacitance per unit volume due to their porous electrode structure compared to electrostatic and electrolytic capacitors. At the macroscopic level, the EC takes the capacitance equation $C = \varepsilon_0 \varepsilon_r A / d$ [6] to the extreme by having a very high electrode surface-area (A) due to the porous electrodes and very small separation d between the electronic and ionic charge at the electrode surface [7]. ε_0 is absolute dielectric constant, and ε_r is relative dielectric constant. The capacitance of large cells, which is about thousands of Farads, allows the storage of Wh energy with voltage limited to 2.7V. The maximum power equation is $P_{\max} = \frac{V^2}{4R}$. Thanks to their very low serial resistance (<1mΩ), they can operate at high levels of instantaneous power [8]. Considerable research is presently being directed towards the development of carbon materials with a tailored pore-size distribution to yield electrodes with high capacitance and low resistance. The incorporation of redox materials (e.g., metal oxides or conducting polymers) into carbon electrodes is also receiving increased attention as a means of increasing capacitance, as is the tailoring of electrodes and electrolytes capable of operating at higher voltages (>3 V). Clearly, the goal is to enhance the specific energy of carbon-based ultra-capacitor [9].

The periods of peak power demand during vehicle acceleration are relatively short, generally less than 30 s. Thus ultra-capacitor can be easily used at these periods to provide the peak power demand. The method used to store energy for ultra-capacitor allows the energy to be stored and released without any chemical reaction taking place, and the ultra-capacitor can accept and release energy fast and with low losses [10, 11]. The combination takes full use of the complementary property of ultra-capacitor and battery.

Some work has started to address this study on the combination of battery and ultra-capacitor [5, 12, 13, 14, 15, 16, 17]. This paper is aimed to explore the energy efficiency of the HESS with the bidirectional DC-DC compared.

Section 2 is about $LiFePO_4$ battery and ultra-capacitor experiment. Section 3 discusses the architecture of the HESS. Section 4 derives the bidirectional DC-DC efficiency equation. Section 5 shows the simulation of the HESS applied in EV. And the last part gives the conclusion. Also, as future research, we will consider modelling the resulting complex power system by using artificial intelligence techniques such as agent based modeling as it has been done in [18] for another complex domain.

2 The energy storage system efficiency experiment

Details follow.

2.1 LiFePO4 battery experiment

$LiFePO_4$ battery is wildly used for its relatively good thermal stability performance. The experiment is implemented on the $LiFePO_4$ battery with nominal capacity 40Ah, under the room temperature 30℃. In the experiment, AeroVironment MT-30 and the environmental chamber are employed.

Figure 1 shows the Hybrid Pulse Power Characterization (HPPC) [19] experiment procedure and result. The maximum pulse discharge current is 90A and the maximum pulse charge current is 85A.

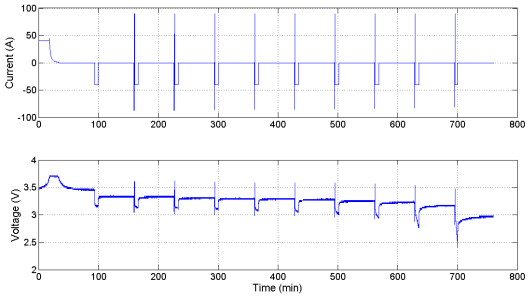

Figure 1 HPPC experiment

The open circuit voltage (Voc) as a function of the State of Charge (SOC) is plotted in Figure 2 based on the HPPC experiment result. The open circuit voltage curve is fitted by smoothing spline with the experimental data.

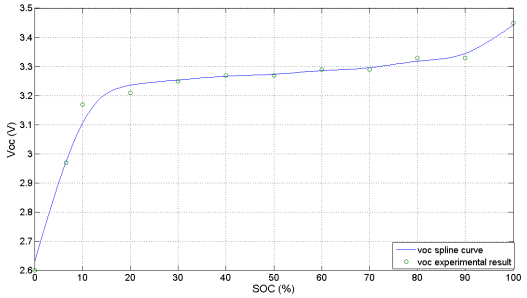

Figure 2 The Open circuit voltage of battery

The battery resistance curve is fitted by two-order polynomial equation with the experimental data,

shown in Figure 3. The resistance coefficients are: p1=2.605e-007; p2 =-3.835e-005; p3 =0.004851.

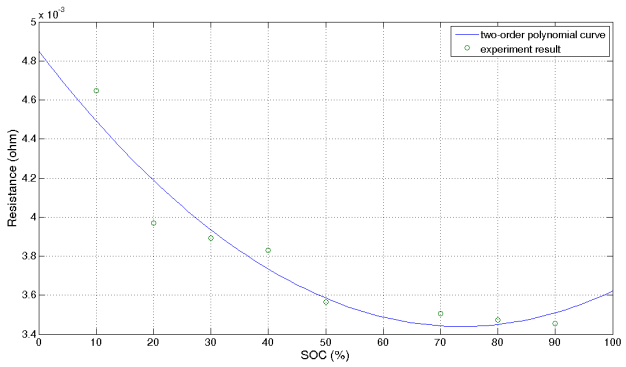

Figure 3 The battery resistance

The two-order polynomial curve:

$$f(SOC) = p1 * SOC^2 + p2 * SOC + p3 \quad (1)$$

The battery discharges at 0.5C, 1C, 1.5C, 2C, 2.5C and 3C current to 2.38v. The Figure 4 shows the discharge curves.

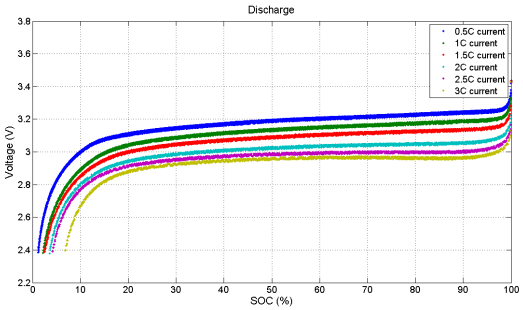

Figure 4 The discharge curves

The battery charges at 0.5C, 1C, 1.5C, and 2C. The Figure 5 shows the charge curves.

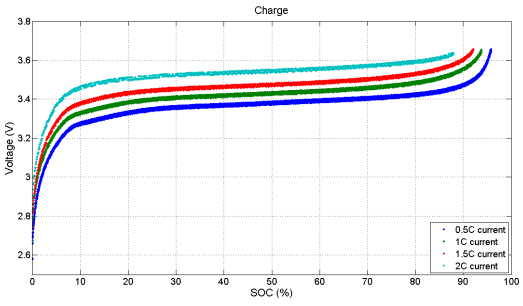

Figure 5 The charge curves

The battery efficiency is:

$$\eta_{discharge} = \frac{V_L(I,T) * I}{Voc * I} = \frac{V_L(I,T)}{Voc} \quad (2)$$

$$\eta_{charge} = \frac{Voc * I}{V_L(I,T) * I} = \frac{Voc}{V_L(I,T)} \quad (3)$$

Where

$V_L(I,T)$ is the battery terminal voltage which is the function of the battery load current I and temperature T;

Voc is the battery open-loop voltage.

The battery discharge efficiency map is shown in Figure 6 and the charge efficiency map is shown in Figure 7.

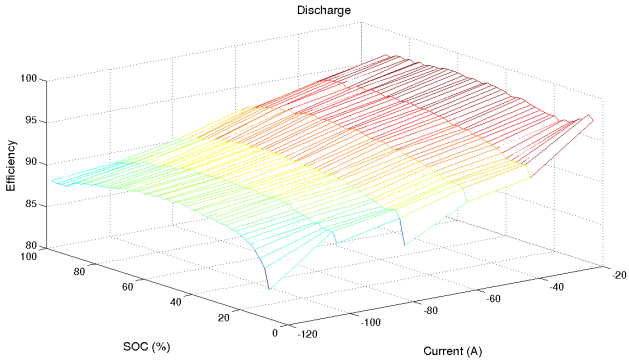

Figure 6 The discharge efficiency

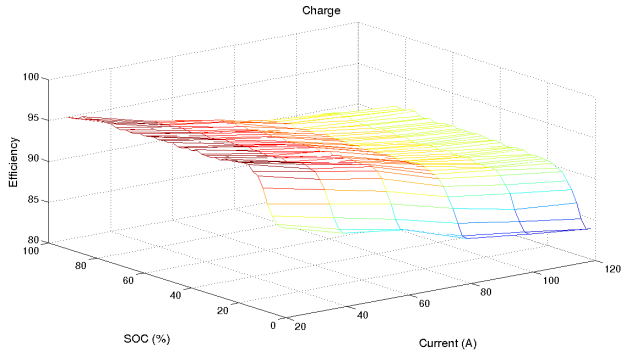

Figure 7 The charge efficiency

Table 2 The battery efficiency results

		Discharge	Charge
0.5C	Max Efficiency(%)	97.7	97.4
	Min Efficiency(%)	93.2	90.9
1.5C	Max Efficiency(%)	94.7	94.5
	Min Efficiency(%)	87.9	87.4
3C	Max Efficiency(%)	90.5	91.4
	Min Efficiency(%)	81	83.5

The battery efficiency results are shown in Table 2. According to the electrochemistry theory, the battery resistance, including the ohm resistance, the electrochemistry polarization resistance and the concentration polarization resistance, increases as the current increases. And this results in the efficiency

decreasing.

2.2 Ultra-capacitor experiment

The ultra-capacitor is Maxwell BMOD0165 P048, and the parameter is shown in Table 3 [20].

Table 3 The ultra-capacitor parameter

Part Number	BMOD0165 P048
Capacitance	165 F
ESR, DC (ohm)	0.0071
Nominal voltage (V)	48

The ultra-capacitor discharges at 50A, 90A, 150A and 250A current to 24v. The experiment is implemented under the room temperature 30℃. The Figure 8 shows the discharge curves.

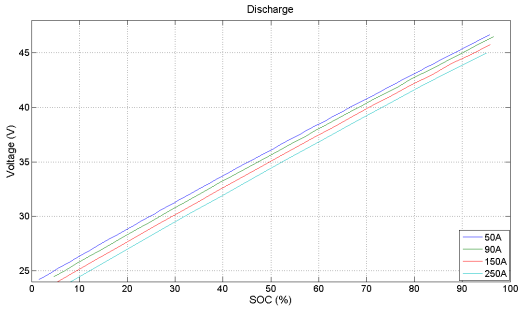

Figure 8 The discharge curves

The ultra-capacitor charges at 50A, 90A, 150A and 250A current to 48v. The Figure 9 shows the charge curves.

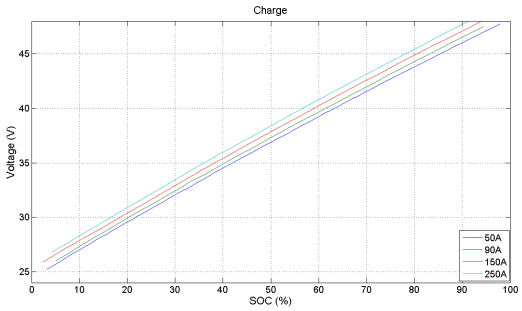

Figure 9 The charge curves

The ultra-capacitor discharge efficiency map is shown in Figure 10 and the charge efficiency map is shown in Figure 11.

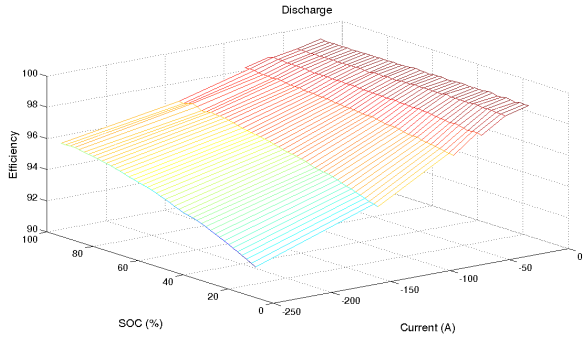

Figure 10 The discharge efficiency

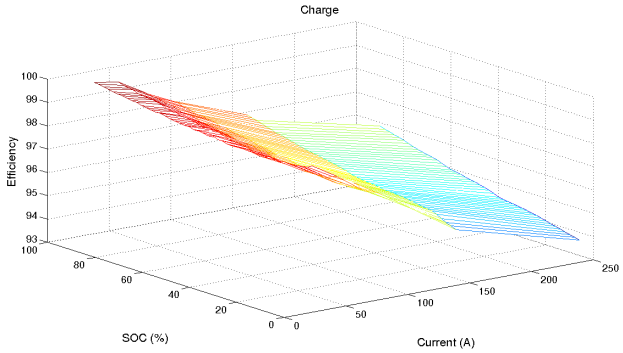

Figure 11 The charge efficiency

The ultra-capacitor efficiency results are shown in Table 4. The ultra-capacitor efficiency decreases as the current increases. Compared with the battery efficiency results shown in Table 2, the ultra-capacitor efficiency is higher than the battery efficiency, especially at the large current. Therefore the proper combination of battery and ultra-capacitor can improve the HESS efficiency by taking use of ultra-capacitor characteristic of high efficiency. However the HESS efficiency is affected by the topology of HESS and the DC-DC converter.

Table 4 The ultra-capacitor efficiency results

		Discharge	Charge
50A	Max Efficiency(%)	99.3	99.6
	Min Efficiency(%)	99	98.2
150A	Max Efficiency(%)	97.4	98.3
	Min Efficiency(%)	93.3	95
250A	Max Efficiency(%)	96	96.2
	Min Efficiency(%)	91.4	93.4

The next section focuses on the topology of HESS and the DC-DC converter efficiency.

3 The HESS design

The important issue is about the topologies of HESS that have been studied over the past years.

Figure 12 shows the diagram of a kind of HESS [21]. By using a bidirectional DC-DC converter to interface the ultra-capacitor, the voltage of the ultra-capacitor can vary in a wide range so the capacitor is fully used. In addition, the nominal voltage of the ultra-capacitor bank can be lower. The battery is connected directly to the DC link; as a result, the DC link voltage can be maintained relatively constant. The main energy source battery directly powers the electric motor.

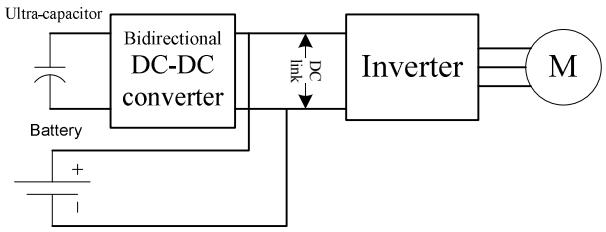

Figure 12 Ultra-capacitor/battery configuration

By switching the position of the battery and ultra-capacitor in Figure 12, the battery/ultra-capacitor configuration as shown in Figure 13 is gotten [22]. In this configuration, the voltage of the battery doesn't relate to the DC link. The ultra-capacitor is connected to the DC link directly working as a low pass filter. The DC link voltage fluctuates in a range to take full use of the ultra-capacitor. The battery powers the electric motor though the DC-DC converter so that the efficiency of the battery is lower than that in Figure 12.

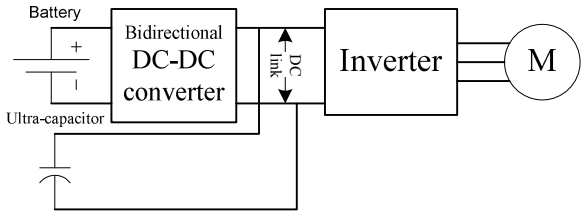

Figure 13 Battery/ultra-capacitor configuration

The multiple converter method parallels the output of the two converters.

Figure **14** shows the diagram of the multiple converter topology [23]. The outputs of the two converters are the same as the DC link voltage. The voltage of both the battery and the ultra-capacitor doesn't relate to the DC link. The disadvantage of this method is that two converters result in the high cost. However, it allows the energy to flow between the sources and a tight control of the DC link voltage [24].

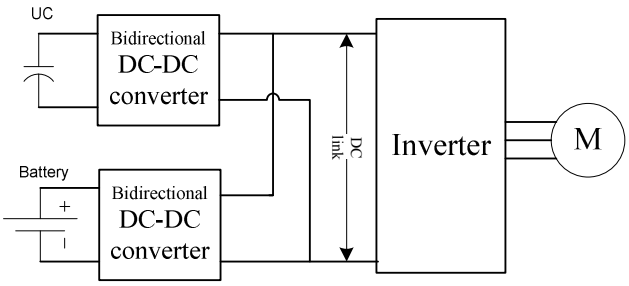

Figure 14 Multiple converter configuration

Another important issue is to find a proper type of DC-DC for HESS. Schupbach and Balda [25] discuss the development of a 35kW half bridge dc-dc converter as the best choice for this application by placing special emphasis on the stress levels that the wide input voltage swing will have on the converter components. Their conclusion: the half bridge, inductor input converter is optimum for such use. The inductor input, single phase leg, mid-point or half bridge converter is the best option for a non-isolated, bi-directional, buck-boost converter to interface an ultra-capacitor to the battery [14].

The architecture of the ultra-capacitor and battery and the inductor input half bridge bidirectional converter is shown as Figure 15. It is composed of the insulated gate bipolar transistor (IGBT) S1 and S2, an inductor L, and an output capacitor C. D1 works as a freewheeling diode under the boost mode to output the energy. D2 works as a freewheeling diode under the buck mode.

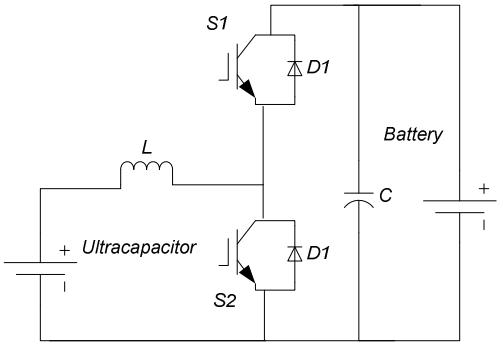

Figure 15 The bidirectional converter in HESS

The voltage level of ultra-capacitor and battery are different. The battery side connected to the motor by inverter is the high voltage level side, and the ultra-capacitor voltage level is relatively low. The ultra-capacitor consists of 4 BMOD0165 P048 in series, and the battery consists of 88 cells in series. The detailed parameter is shown in table 5.

Table 5 The HESS parameter

Part Number	Ultra-capacitor 4 BMOD0165 P048 in series	Battery 88 cells in series
Capacitance	41 F	40 Ah
ESR, DC (ohm)	0.0284	0.264
Nominal voltage (V)	192	290

4 The bidirectional DC-DC efficiency analysis

The bidirectional DC-DC is designed to work on the continuous current mode. The bidirectional DC-DC efficiency as a function of the current and voltage of the ultra-capacitor, and the battery voltage is derived in the stable state.

4.1 Boost operation

The equivalent circuits of continuous current DC-DC converter are shown in Figure 16. The state equations of the equivalent circuits are shown in Eqs. (4) and (5).

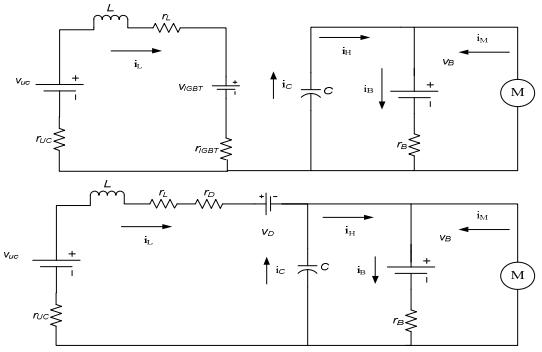

Figure 16 The equivalent circuit of boost operation

The state equation for the first equivalent circuit at boost operation is:

$$\begin{bmatrix} \frac{di_L}{dt} \\ \frac{dv_C}{dt} \end{bmatrix} = \begin{bmatrix} -(r_{UC}+r_L+r_{IGBT})/L & 0 \\ 0 & -\frac{1}{r_B C} \end{bmatrix} \begin{bmatrix} i_L \\ v_C \end{bmatrix} + \begin{bmatrix} 1/L & 0 & 0 \\ 0 & \frac{1}{r_B C} & 1/C \end{bmatrix} \begin{bmatrix} v_{UC} \\ v_B \\ i_M \end{bmatrix} - \begin{bmatrix} v_{IGBT}/L \\ 0 \end{bmatrix} \quad (4)$$

The state equation for the second equivalent circuit at boost operation is:

$$\begin{bmatrix} \frac{di_L}{dt} \\ \frac{dv_C}{dt} \end{bmatrix} = \begin{bmatrix} -(r_D+r_{UC}+r_L)/L & -1/L \\ 1/C & -\frac{1}{r_B C} \end{bmatrix} \begin{bmatrix} i_L \\ v_C \end{bmatrix} + \begin{bmatrix} 1/L & 0 & 0 \\ 0 & \frac{1}{r_B C} & 1/C \end{bmatrix} \begin{bmatrix} v_{UC} \\ v_B \\ i_M \end{bmatrix} - \begin{bmatrix} v_D/L \\ 0 \end{bmatrix} \quad (5)$$

Where

D: "Duty cycle" of the pulse width modulation applied to IGBT.

R_X: Equivalent series resistance of battery, ultra-capacitor, inductor or diode.

V_X: Battery voltage, ultra-capacitor voltage or IGBT drop.

Eq (4) is simplified as $\frac{dx}{dt} = A_1 x + B_1 V + C_1$.

Eq (5) is simplified as $\frac{dx}{dt} = A_2 x + B_2 V + C_2$.

To simplify the model, it is assumed that the average value of the voltage in the inductance L in one period of time is approximately zero [8]. Another important assumption is that the initial voltage in the capacitor C is equal to the voltage at the end in one period. These assumptions are expressed as Eq (6).

$$\int_t^{t+Ts} \frac{dx}{dt} = 0 \quad (6)$$

The average state equation (7) is derived by Eqs. (4), (5) and (6).

$$D\left(A_1 X + B_1 V + C_1\right) + D'\left(A_2 X + B_2 V + C_2\right) = 0 \quad (7)$$

Where $D' = 1 - D$

The Eq. (8) is the solution of Eq. (7).

$$\begin{cases} D = \dfrac{v_D + r_B i_M + v_B - v_{IGBT} + (r_D - r_{IGBT} + 2r_B) I_L \pm \sqrt{\left[v_D + r_B i_M + v_B - v_{IGBT} + (r_D - r_{IGBT} + 2r_B) I_L\right]^2 - 4r_B I_L \left[(r_D + r_B + r_L + r_{UC}) I_L - v_{UC} + r_B i_M + v_B + v_D\right]}}{2r_B I_L} \\ v_C = r_B (1-D) I_L + v_B + r_B i_M \\ D \subset (0,1) \end{cases} \quad (8)$$

The efficiency of the stable state is:

$$\eta_{Boost} = \frac{V_H I_H}{(v_{UC} - r_{UC} I_L) I_L} = \frac{V_C (1-D) I_L}{(v_{UC} - r_{UC} I_L) I_L} \quad (9)$$

The DC-DC parameter is listed in Table 6 in detail.

Table 6. DC-DC parameter

Part	parameter	
Inductor L	Inductance (μH)	150
	ESR (ohm)	0.037
IGBT	The internal resistance (ohm)	2.3e-3
	Forward voltage (V)	0.7
Diode	The internal resistance (ohm)	3e-3
	Forward voltage (V)	0.8

Figure 17 shows when i_M=-160A and V_{uc}=192v, the efficiency changes with V_b and I_L. The efficiency slight changes with V_B. And as I_L increases, the efficiency decreases.

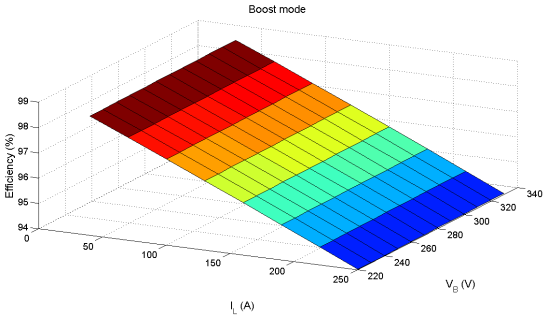

Figure 17 The boost efficiency changes with V_B and I_L

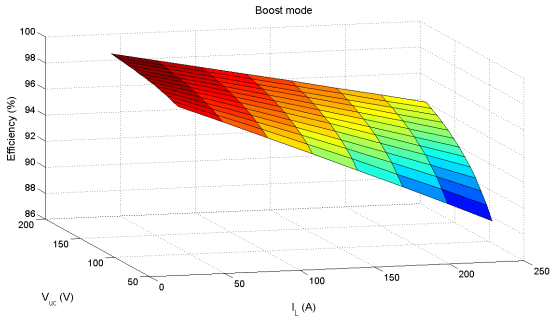

Figure 18 The boost efficiency changes with V_{uc} and I_L

Figure 18 shows when i_M=-160A and V_B=290.4V, the efficiency changes with V_{uc} and I_L. As I_L increases and V_{uc} decreases, the efficiency decreases.

4.2 Buck operation

The equivalent circuits of buck operation are shown in Figure 19.

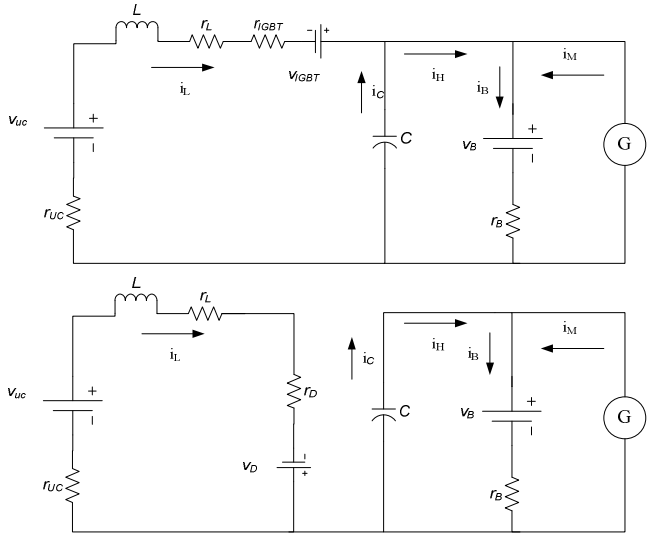

Figure 19 the equivalent circuit of buck operation

The state equation for the first equivalent circuit at buck operation is:

$$\begin{bmatrix} \frac{di_L}{dt} \\ \frac{dv_C}{dt} \end{bmatrix} = \begin{bmatrix} -(r_{IGBT}+r_{UC}+r_L)/L & -1/L \\ 1/C & -\frac{1}{r_B C} \end{bmatrix} \begin{bmatrix} i_L \\ v_C \end{bmatrix} + \begin{bmatrix} 1/L & 0 & 0 \\ 0 & \frac{1}{r_B C} & 1/C \end{bmatrix} \begin{bmatrix} v_{UC} \\ v_B \\ i_M \end{bmatrix} + \begin{bmatrix} v_{IGBT}/L \\ 0 \end{bmatrix} \quad (10)$$

The state equation for the second equivalent circuit at buck operation is:

$$\begin{bmatrix} \frac{di_L}{dt} \\ \frac{dv_C}{dt} \end{bmatrix} = \begin{bmatrix} -(r_{UC}+r_L+r_D)/L & 0 \\ 0 & -\frac{1}{r_B C} \end{bmatrix} \begin{bmatrix} i_L \\ v_C \end{bmatrix} + \begin{bmatrix} 1/L & 0 & 0 \\ 0 & \frac{1}{r_B C} & 1/C \end{bmatrix} \begin{bmatrix} v_{UC} \\ v_B \\ i_M \end{bmatrix} + \begin{bmatrix} v_D/L \\ 0 \end{bmatrix} \quad (11)$$

The solution is:

$$\begin{cases} D = \dfrac{(r_{IGBT}-r_D)I_L + v_B + r_B i_M + v_D - v_{IGBT} \pm \sqrt{\left[(r_{IGBT}-r_D)I_L + v_B + r_B i_M + v_D - v_{IGBT}\right]^2 + 4r_B I_L \left[v_{UC} + v_D - (r_{UC}+r_L+r_D)I_L\right]}}{-2r_B i_L} \\ V_C = D r_B I_L + v_B + r_B i_M \\ D \subset (0,1) \end{cases} \quad (12)$$

The efficiency equation is:

$$\eta_{Buck} = \frac{(v_{UC} - r_{UC} I_L) I_L}{V_C I_H} \quad (13)$$

Figure 20 shows when i_M=150A and V_{uc}=192v, the efficiency changes with V_B and I_L. The efficiency slight change with V_b. And as I_L increases, the efficiency decreases.

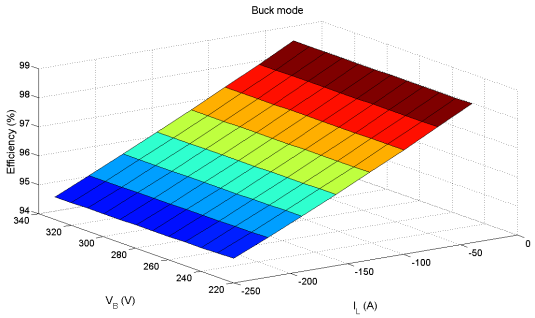

Figure 20 The buck efficiency changes with V_B and I_L

Figure 21 shows when i_M=150A and V_B=290.4V, the efficiency changes with V_{uc} and I_L. As I_L increases and V_{uc} decreases, the efficiency decreases.

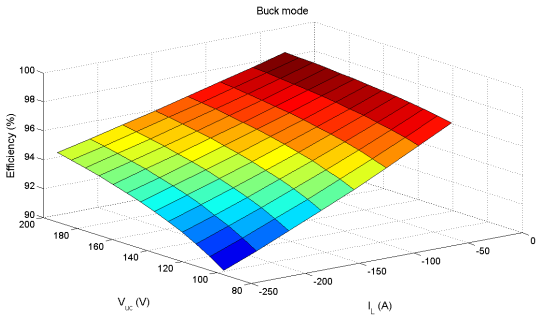

Figure 21 The buck efficiency

In the next section, the simulation will be done to research on the HESS based on the efficiency maps of ultra-capacitor, $LiFePO_4$ battery and DC-DC converter.

5 Simulation Results

The EV with HESS is designed shown in Figure 22. The front wheels are driven by an electric motor.

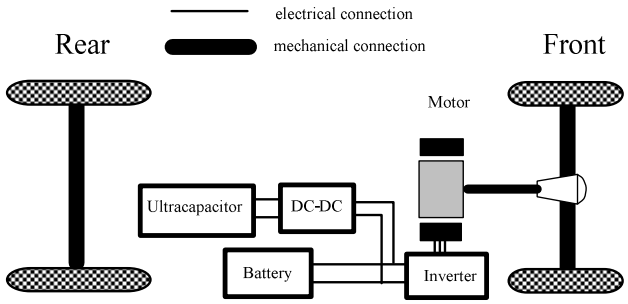

Figure 22 The EV with HESS

Based on AVL cruise software, the vehicle simulation is done for the EV. The vehicle parameters are shown in Table 7. The AVL Cruise simulation schema is shown in Figure 23.

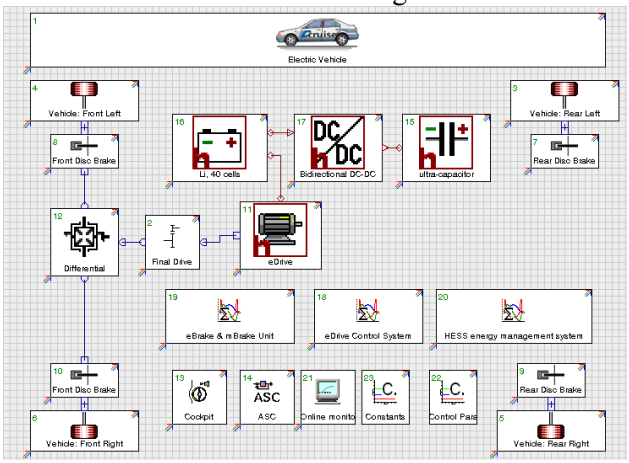

Figure 23 The AVL Cruise simulation schema

The NEDC cycle shown in Figure 24 is chosen to simulate the vehicle fuel economy. The simulation result of the electrical power is shown in Figure 24. The electrical power reaches the maximum in acceleration mode and regenerative braking mode. The maximum acceleration power reaches to 39.4 kW. The constant driving power at 50 km/h is 4.7kW and that at 120 km/h is 27.8 kW. The peak power in acceleration is much higher than the power in constant driving mode.

Table 7 Vehicle parameters

Curb/Gross weight (kg)	1200/1580
Wheel base (m)	2.467
Frontal area (m^2)	1.97
Aerodynamic drag coefficient	0.284
Rolling resistance coefficient at 120km/h velocity	0.0139
Tire rolling radius (m)	0.301

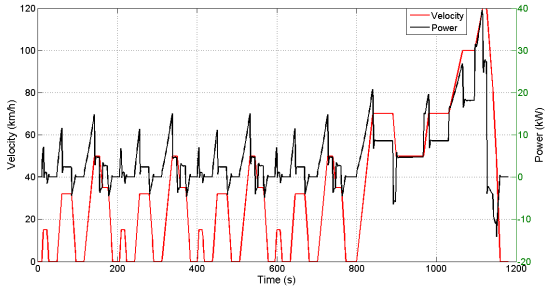

Figure 24 NEDC cycle and the electrical power

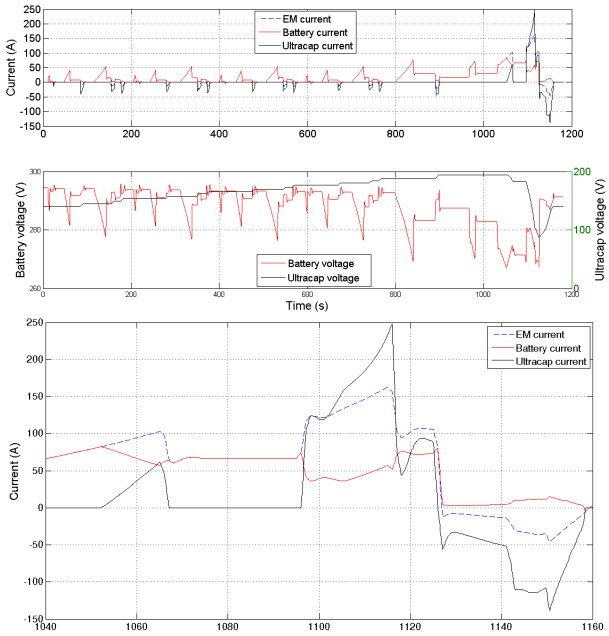

Figure 25 Battery plus ultra-capacitor in HESS

The maximum motor current is 162.7A, as shown in Figure 25. In HESS, the maximum discharging current of battery is 82.3A, and that of ultra-capacitor is 248.3A. In regenerative braking mode, the maximum motor current is 46A, and the maximum charging current of battery is 7A and that of ultra-capacitor is 138A. With the ultra-capacitor's support, the maximum charging/discharging current of battery decreases. The ultra-capacitor voltage at the beginning of the cycle is equal to that at the end, and is charge balance.

The voltage range of DC link in HESS is from 295.7 V to 267 V and that in battery only system is from 305.3 V to 242.1 V shown in Figure 26. The

voltage variation of the DC link in HESS is less than that in the battery only system. The HESS is benefit to minimize the voltage variation of the DC link.

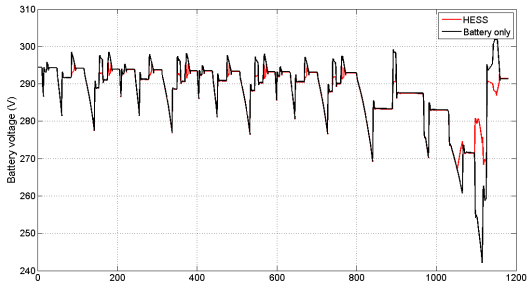

Figure 26 The comparison of DC link voltage in battery only system and in HESS

The efficiency of ultra-capacitor plus DC-DC in HESS is shown in Figure 27 and the comparison of battery efficiency in battery only system and in HESS is shown in Figure 28. The energy management strategy of the HESS is to limit the battery max current ratio to 2C. Therefore with the ultra-capacitor's support, the battery is relieved from the stress of peak power and the results verify that the efficiency of the battery is improved.

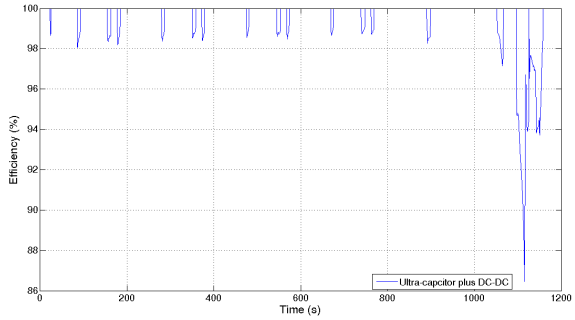

Figure 27 The efficiency of ultra-capacitor plus DC-DC in HESS

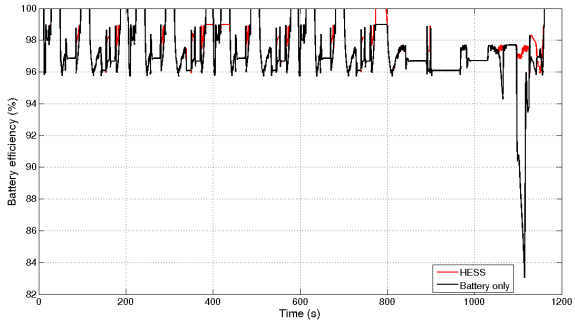

Figure 28 The comparison of battery efficiency in battery only system and in HESS

The battery energy consumption under the NEDC cycle is shown in Figure 29. The ultra-capacitor is used to absorb the regenerative braking energy. Therefore the battery energy consumption in HESS is more than that in battery only system before the 1100 second of the cycle. The total energy consumption under the NEDC cycle in battery only system is 1.664 kWh and that in HESS is 1.606 kWh. Compared to the battery only system, the energy efficiency improvement in HESS is 3.5%.

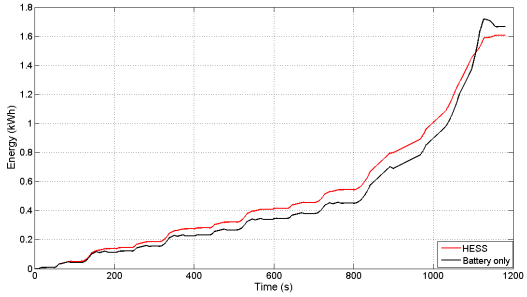

Figure 29 The comparison of energy consumption in battery only system and in HESS

6 Conclusion

The present paper explores the energy improvement of the proper combination of $LiFePO_4$ battery and ultra-capacitor compared with $LiFePO_4$ battery only system, taking into account of the DC-DC converter efficiency. Based on the efficiency experiment of ultra-capacitor and $LiFePO_4$ battery, the ultra-capacitor efficiency is higher than the battery efficiency, especially at the large current. A review of the most widely used HESS topologies is given. The inductor input half bridge bidirectional converter is employed as the interface of the ultra-capacitor and battery Based on the architecture, the DC-DC model has been built to acquire the bidirectional DC-DC efficiency map. The bidirectional DC-DC efficiency is derived in the stable state. It doesn't take the transient response into consideration. However, the switching frequency of DC-DC converter is more than 10 kHz. And the response time is in millisecond magnitude. Therefore the transition process isn't considered in the energy efficiency evaluation of the driving cycle in this paper.

Finally, the simulation results demonstrate that compared with the battery only system, the EV with the HESS is more efficient and the energy efficiency improvement is 3.5%. The voltage variation of the DC link in HESS is less than that in the battery only system. The energy management strategy optimization of HESS is the future direction of the present research.

References:

[1] W. W. Xiong, Z. W. Wu, C. L. Yin, L. Chen, Economical comparison of three hybrid electric car solutions, *IEEE Vehicle Power and Propulsion Conference*, 2008.

[2] P. Z. Zhang, C. L. Yin, Y. Zhang, Z. W. Wu, Optimal energy management for a complex hybrid electric vehicle: Tolerating power-loss of motor, *Journal of Shanghai Jiaotong University (Science)*, Vol.14, No.4, 2009, pp.476-481.

[3] Y. J. Huang, C. L. Yin, J. W. Zhang, Optimal Torque Distribution Control Strategy for Parallel Hybrid Electric Urban Buses *WSEAS TRANSACTIONS on SYSTEMS*, Vol.7, No.6, 2008, pp.758-773.

[4] W. W. Xiong, C. L. Yin, Design of Series-parallel Hybrid Electric Propulsion Systems and Application in City Transit Bus. *WSEAS TRANSACTIONS on SYSTEMS*, Vol.8, No.5, 2009, pp.578-590.

[5] J. M. Miller, U. Deshpande, T. J. Dougherty, T. Bohn, Power Electronic Enabled Active Hybrid Energy Storage System and its Economic Viability, *Applied Power Electronics Conference and Exposition*, 2009, pp.190-198.

[6] R. Kötz, M. Carlen, Principles and applications of electrochemical capacitors, *Electrochim*, Acta 45, 2000, pp.2483-2498.

[7] P. Sharma, T. S. Bhatti, A review on electrochemical double-layer capacitors, *Energy conversion and Management*, Vol.51, No.12, 2010, pp.2901-12.

[8] W. Lajnef, J. M. Vinassa, O. Briat, S. Azzopardi, E. Woirgard, Characterization methods and modelling of ultracapacitors for use as peak power sources, *Journal of Power Sources*, Vol.168, No.2, 2007, pp. 553-560.

[9] A. G. Pandolfo, A. F. Hollenkamp, (2006). Carbon properties and their role in supercapacitors, *Journal of Power Sources*, Vol.157, No.1, 2007, pp.11-27.

[10] H. Farzanehfard, D. S. Beyragh, E. Adib, A bidirectional soft switched ultracapacitor interface circuit for hybrid electric vehicle, *Journal of Energy Conversion and Management*, Vol. 49, 2008, pp. 3578-3584.

[11] J. W. Dixon, M. E. Ortlizar, Ultracapacitors + DC–DC converters in regenerative braking system, *IEEE Aerospace and Electronic Systems Magazine*, Vol.17, 2002, pp:16-21.

[12] J. M. Miller, Trends in Vehicle Energy Storage Systems: Batteries and Ultracapacitors to Unite, *IEEE Vehicle Power and Propulsion Conference, VPPC 2008*, Harbin, 2008.

[13] C. Jian, A. Emadi, A new battery/ultra-capacitor hybrid energy storage system for electric, hybrid and plug-in hybrid electric vehicles, *IEEE Vehicle Power and Propulsion Conference, VPPC 2009*, 2009, pp:941-946.

[14] J. M. Miller, G. Sartorelli, Battery and ultracapacitor combinations-Where should the converter go? *IEEE Vehicle Power and Propulsion Conference, VPPC 2010*, 2010.

[15] I. D. Oltean, A modality to improve the dynamic behavior for power supply or for batteries. Proceedings of the *14th WSEAS international system, Latest Trends on Systems*, Vol.2, 2010, pp:626-629

[16] J. Lopes, J. C. Quadrado, Dual Mode Hybrid Bus Energy Storage System,WSEAS Transactions on Systems, 2004.

[17] Z. W. Wu, Z. L. Zhang, C. L. Yin, Z. Zhao, Design of a soft switching bidirectional DC-DC power converter for ultracapacitor-battery interfaces, International Journal of Automotive Technology, Vol.13, No.2, 2012, pp.325-336.

[18] F. Neri, A Comparative Study of a Financial Agent Based Simulator Across Learning Scenarios, *In Agents and Data Mining Interaction, Lecture Notes in Computer Science*, Vol. 7103, 2012, pp.86-97.

[19] PNGV Battery Test Manual, DOE/ID-10597, Revision 3, February 2001.

[20] Maxwell Technologies. Maxwell Technologies BMOD0165-48.6V [OL], http://www.maxwell.com/products/ultracapacitors/product.aspx?PID=48V-MODULES.

[21] J. Moreno, M. E. Ortuzar, J. W. Dixon, Energy-management system for a hybrid electric vehicle, using ultracapacitors and neural networks, *IEEE Transactions on Industrial Electronics*, Vol. 53, 2006, pp: 614-623.

[22] L. Gao, R. A. Dougal, S. Liu, Power enhancement of an actively controlled battery/ultracapacitor hybrid, *IEEE Transactions on Power Electronics*, Vol. 20, 2005, pp:236-243.

[23] A. Di Napoli, F. Crescimbini, F. Guilii Capponi, L. Solero, Control strategy for multiple input DC-DC power converters devoted to hybrid vehicle propulsion systems, *IEEE International Symposium on Industrial Electronics*, ISIE 2002, 2002, pp. 1036-1041.

[24] R. de Castro, J. P. Trovão, P. Pacheco, P. Melo, P. G. Pereirinha, R. E. Araujo, DC Link Control for Multiple Energy Sources in Electric Vehicles,

IEEE Vehicle Power and Propulsion Conference, 2011.

[25] R. M. Schupbach, J. C. Balda, 35kW Ultracapacitor unit for Power Management of Hybrid Electric Vehicles: Bi-directional dc-dc Converter Design, *The 35th IEEE Power Electronics Specialists Conference*, PESC2004, Aachen, Germany, 2004.